Supporting Information

Synergistic effect of two actions sites on nitrogen-doped carbon catalyst towards acetylene hydrochlorination

Bolin Wang,[1,2] Yuxue Yue,[1] Xiangxue Pang,[1] Wenrui Zhu,[1] Zhi Chen,[1] Shujuan Shao,[1] Ting Wang,[1] Zhiyan Pan,[2] Xiaonian Li[1,*] and Jia Zhao[1,*]

[1] Industrial Catalysis Institute of Zhejiang University of Technology, Hangzhou, 310014, People's Republic of China

[2] Department of Environmental Engineering, Zhejiang University of Technology, Hangzhou, 310014, People's Republic of China

* Corresponding author. Tel: +86 571 88320002. E-mail: xnli@zjut.edu.cn (Xiaonian Li)

* Corresponding author. Tel: +86 571 88871656. E-mail: jiazhao@zjut.edu.cn (Jia Zhao)

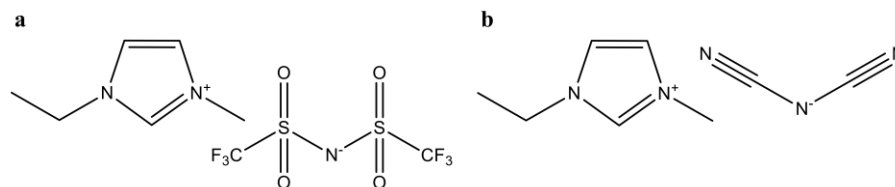# 1. Experimental Section

1.1 Catalyst preparation

Fig. S1.1-1 The structure of the selected ILs: (a) [EMIM][NTf$_2$] and (b) [EMIM][N(CN)$_2$].

Ionic liquids (ILs) 1-ethyl-3-methylimidazolium-bis (trifluoromethylsulfonyl) imide [EMIM][NTf$_2$] and 1-ethyl-3-methylimidazolium dicyanamide [EMIM][N(CN)$_2$], (Lanzhou Greenchem. ILS, LICP. CAS., Fig. S1.1-1) were mixed together at 50 °C in an aqueous solution of ethanol at a molar ratio of 5:1 [EMIM][NTf$_2$]: [EMIM][N(CN)$_2$]. The obtained binary IL-mixture was carbonized at 1000, 900, 700, and 600 °C under nitrogen (N$_2$) atmosphere to synthesize carriers named NC1000, NC900, NC700 and NC600, respectively. Because of the [N(CN)$_2^-$] nitrile-containing anions in [EMIM][N(CN)$_2$], a carbonization yield of 17.52 wt.% was observed. The carbon material synthesized here presents high mechanical strength with a slight change during reaction process, which is stable at about ~91%. All prepared carriers were carefully ground to pass through a 120 mesh before use.

1.2 Catalytic reaction evaluation

Catalytic performance of acetylene hydrochlorination was carried out in a continuous-flow fixed-bed micro-reactor (Fig. S1.2-1). Firstly, the reactor containing catalyst at 180 °C was flushed using nitrogen gas for 0.5 h. Then, reaction gas mixture of C$_2$H$_2$ and HCl was fed into the cleaned reactor at a gas hourly space velocity of C$_2$H$_2$

(GHSV) of 90 h^{-1}, C_2H_2 : HCl ratio was kept constant at a value of 1 : 1.2. The exiting gas from the reactor was passed through a saturated NaOH solution in an absorption bottle to remove any unreacted HCl before it was sent to be analyzed by an online gas chromatography (GC 9790, Zhejiang Fuli Analytical Instruments Co., Ltd.). According to Weisz-Prater Criterion and Mears Criterion, the internal and external mass transfer limitations were insignificant and related experiments were excluded (Section 2 of *Supporting Information* for more details). The reaction rate (r) was calculated as:

$$r=\frac{n_{C2H2}^{inlet}-n_{C2H2}^{outlet}}{t_R \times W_{Cat}}$$

Where $r\left(mol_{C2H2} \cdot h^{-1} \cdot kg_{Cat}^{-1}\right)$ is the reaction rate, n_{C2H2}^{inlet} (mol) and n_{C2H2}^{outlet} (mol) is the respective molar flows of acetylene, t_R. is reaction time (h), W_{Cat} is the mass content of evaluated catalysts.
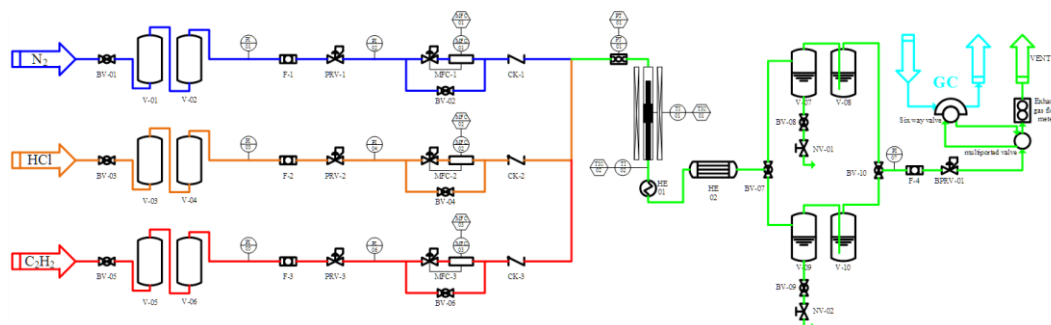

Fig. S1.2-1 Schematic representation of the experimental rig as applied in the here reported continuous flow, gas phase acetylene hydrochlorination experiments.

1.3 Characterization of catalysts

Nitrogen adsorption/desorption isotherms were acquired at 77 K using an ASAP 2020 micromeritics gas adsorption analyzer. X-ray photoelectron spectroscopy (XPS) was conducted using a Kratos AXIS Ultra DLD spectrometer. The samples were analyzed at an electron take-off angle of 45° and a pass energy of 46.95 eV. Energy

dispersive analysis of X-rays (EDX) was carried out on a Tecnai G2 F30 S transmission electron microscope operating at 200 keV. Temperature-programmed desorption (TPD) of the sample and mass spectrometry (MS) analysis of the generated gas were measured on an Omnistar GSD320 mass spectrometer. For Individual C_2H_2-TPD, the sample (100 mg) was loaded into an U-shaped quartz micro-reactor, pretreated in Ar (25 cm^3 min^{-1}) at 673 K for 2 h, and cooled to 373 K. Individual C_2H_2 (10 cm^3 min^{-1}) was then repeatedly injected with a loop until the catalyst was saturated with C_2H_2. This step in the experiment lasted about two hours. After purging in Ar (20 cm^3 min^{-1}) at reaction temperature for 2 h, the desorption was initiated by increasing the temperature from 373 to 673 K using a ramp of 10 K min^{-1}, while monitoring the desorbed C_2H_2, using a Omnistar GSD320 mass spectrometer. Individual HCl-TPD was conducted in the same way with pure HCl (10 cm^3 min^{-1}) as the pretreating gas. Quantitative analysis of gas is to establish the relationship between gas molar and signal peak area by injecting the gas with known content into the detector, and to determine the conversion coefficient. In order to ensure the repeatability of the data, the conversion coefficient is the average value obtained by many groups of experiments. For gas mixture of reaction gas [C_2H_2 + HCl], C_2H_2-TPD, the sample (100 mg) was loaded into an U-shaped quartz micro-reactor, pretreated in Ar (25 cm^3 min^{-1}) at 673 K for 2 h, and cooled to 373 K. Reaction gas [C_2H_2 + HCl] (10 cm^3 min^{-1}) was then repeatedly injected with a loop until the catalyst was saturated with [C_2H_2 + HCl]. This step in the experiment lasted about two hours. After purging in Ar (20 cm^3 min^{-1}) at reaction temperature for 2 h, the desorption was initiated by increasing the temperature from 373 to 673 K using a ramp of 10 K

min^{-1}, while monitoring the desorbed C_2H_2, using a Omnistar GSD320 mass spectrometer. Quantitative analysis of gas is to establish the relationship between gas molar and signal peak area by injecting the gas with known content into the detector, and to determine the conversion coefficient. In order to ensure the repeatability of the data, the conversion coefficient is the average value obtained by many groups of experiments. Raman spectroscopy was carried out in a WITec CRM 200 confocal Raman microscope with a 532 nm diode laser. FT-IR characterizations were performed on a Nicolet 6700. Calculations of the energies and structures were performed using the density functional theory (DFT) with the ADF-BAND package and the Perdew-Burke-Ernzerhof (PBE) functional and scalar relativistic corrections. Meanwhile, a DZP and a TZP basis set were used for valence orbitals and Pd, respectively. The self-consistent field and gradients were converged to 10^{-5} Hartree and 0.001 Hartree/Å, respectively. Default parameters were used for the rest of the settings.

2. Internal and external mass transfer limitations

2.1 Internal Diffusion: Weisz-Prater Criterion

The absence of internal mass transfer limitations was evaluated using the Weisz-Prater criterion [S1-S2], where if C_{WP} is lower than 1, the internal mass transfer effects can be neglected:

$$C_{WP} = \frac{-r'_{A(obs)}\rho_c R^2}{D_e C_{AS}} < 1 \qquad (S. 1)$$

$-r'_{A(obs)} =$ Observed reaction rate: 5.94 mol·h^{-1}kg$_{Cat}^{-1}$

$\rho_c =$ Solid catalyst density: 400 kg^{-3}

$R =$ Particle radius: $9\cdot10^{-5}$ m

C_{AS} = Concentration of reaction gas at the surface of the catalyst. C_{AS} = $1.4 \cdot 10^{-2}$ kmol·m^{-3}

D_e = Effective gas-phase diffusity [S1]:

$$D_e = \frac{D_{AB} \varepsilon_p \sigma_c}{\tau} \tag{S. 2}$$

D_{AB} = Gas-phase diffusivity. D_{AB} for a mixture was calculated according to Perry's Chemical Engineer's Handbook [S2] to be $12.56 \cdot 10^{-5}$ m^2/s

ε_p = Pellet porosity = 0.5, σ_c = Constriction factor = 0.6, τ = Tortuosity = 3, D_e = $1.256 \cdot 10^{-5} \ m^2 \cdot s^{-1}$

Solving equation (S. 1)

$$C_{WP} = \frac{1.65 \cdot 10^{-6} \ kmol \ s^{-1} \cdot kg_{Cat}^{-1} \cdot 400 \ kg_{Cat} m^{-3} \ (\cdot 9 \cdot 10^{-5} \ m)^2}{1.256 \cdot 10^{-5} \ m^2 s^{-1} \cdot 1.4 \cdot 10^{-2} \ kmol \ m^{-3}} = 3.04 \cdot 10^{-5} \ll 1$$

Therefore, this system does not suffer from internal mass transfer limitations.

2.2 External Diffusion: Mears Criterion

The absence of external mass transfer limitations can be evaluated using the Mears criterion:

$$\frac{-r'_A \rho_b R n}{k_c C_{Ab}} < 0.15 \tag{S. 3}$$

$-r'_{A(obs)}$ = Observed reaction rate: 5.94 mol·h^{-1}kg$_{Cat}^{-1}$

ρ_b = bulk density of the catalyst bed: 400 kg·m^{-3}

R = Particle radius: $9 \cdot 10^{-5}$ m

n = reaction order If n = 2 (Real reaction order n < 2)

C_{Ab} = Concentration of reaction gas at the surface of the catalyst. C_{AS} = $1.4 \cdot 10^{-2}$ kmol·m^{-3}

k_c = mass transfer coefficient (m s^{-1}) = 0.14 m s^{-1}

k_c can be calculated from the Sherwood number

$$Sh = \frac{k_c d_p}{D_A} = 0.91 \cdot 0.91 \cdot Re^{0.49} \cdot Sc^{1/3} \tag{S. 4}$$

Solving equation (S.3):

$$\frac{1.65 \cdot 10^{-6} kmol \; s^{-1} \cdot kg_{Cat}^{-1} \cdot 400 kg_{Cat} m^{-3} \cdot 3 \cdot 10^{-5} m \cdot 2}{0.14 m \cdot s^{-1} \cdot 1.4 \cdot 10^{-2} kmol \; m^{-3}} = 1.05 \cdot 10^{-5} \ll 0.15$$

Therefore, this system does not suffer from external mass transfer limitations.

3. Catalytic behavior of the graphitic N/pyridinic N^+O configurations

3.1 Reactants adsorption properties

In this work, both pyrrolic N and pyridinic N were decomposed at 1000 °C, leaving only graphitic N and pyridinic N^+O^- configurations in NC1000. The reaction rates were estimated as 4.96, 5.94, 2.39 and 0.13 $mol_{C_2H_2} h^{-1} kg_{Cat}^{-1}$ for NC600, NC700, NC900 and NC1000, respectively (Fig. 1d). Although the catalytic activity of NC1000 was very little in comparison with NC600-900, the possible catalytic mechanism of NC1000 was also studied. Generally, the reaction is triggered from the adsorption and activation of the reactants. Therefore, we first studied the adsorption properties of C_2H_2 and HCl on NC1000.
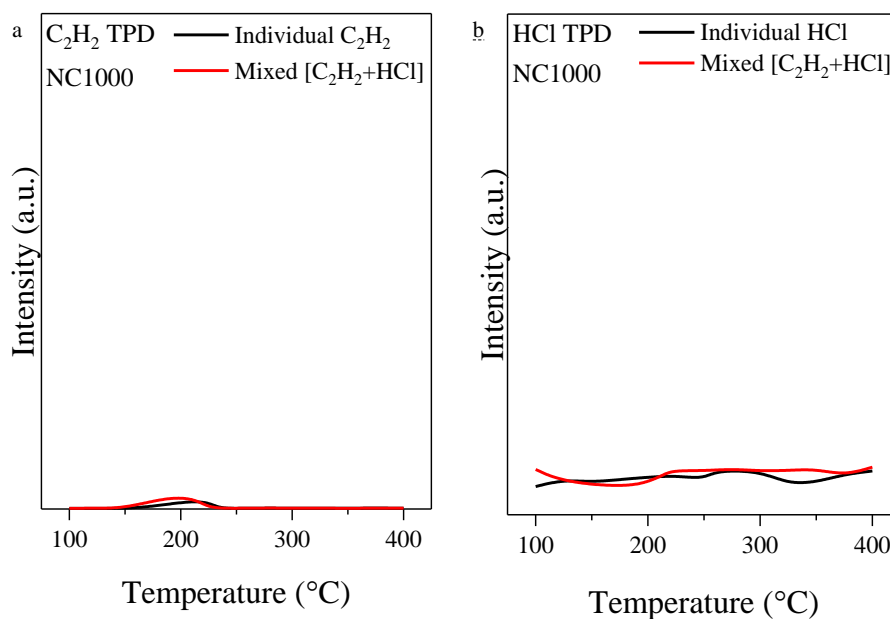
Fig. S3.1-1 C_2H_2 and HCl TPD-MS of NC1000 under individual C_2H_2/HCl, and gas mixture of [C_2H_2 + HCl] pretreatment.

From Fig. S3.1-1, NC1000 shown weak C_2H_2 adsorption capacity and almost no adsorption for HCl. At the same time, the amount of C_2H_2 adsorption was much smaller than NC600-900 catalysts (Fig. S6 in section 4 of *Supporting Information*). This result explained why the catalytic activity of NC1000 was the lowest in the evaluated NCT (T=600-1000) catalysts under the same reaction conditions. This also means that the catalytic activity of the graphitic N and pyridinic N^+O^- in NC1000 surface is not high, compared to pyrrolic N and pyridinic N configurations.
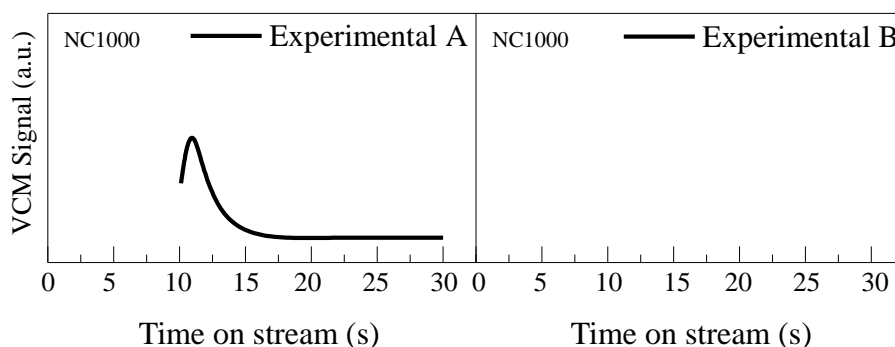
3.2 Possible reaction pathway

Fig. S3.2-1 MS signals of VCM for NC600, NC700 and NC900 under different reaction conditions:

Experiental A: C_2H_2 (30 min) $\rightarrow$ N_2 (60 min) $\rightarrow$ HCl $\rightarrow$ VCM Signal

Experiental B: HCl (30 min) $\rightarrow$ N_2 (60 min) $\rightarrow$ C_2H_2 $\rightarrow$ VCM Signal

In experimental A (**B**), the evaluated sample was first pre-treated with C_2H_2 (**B, HCl**) under reaction conditions for 30 min, followed by N_2 purging for 60 min to remove the physically adsorbed C_2H_2 (**B, HCl**) residual in the catalyst bed. Subsequently, HCl (**B, C_2H_2**) was introduced into the catalyst bed to detect the signal of VCM.

We designed the above experiment to study the possible reaction pathway of NC1000 in acetylene hydrochlorination. VCM signal can only be detected in Experimental A. In Experimental B, no VCM signal has been found which was consistent with the HCl-TPD results in Fig. S3.1-1, since the NC1000 did not have the ability to adsorb and active HCl. The presentation of this experimental result means that this reaction can only be performed in the following ways: gaseous HCl reacted with the adsorbed C_2H_2 to generate VCM, following the typical Eley-Rideal mechanism.

3.3 DFT calculations

Although several methods of synthesizing N-doped carbon materials have been developed, multiple types of N configurations are usually introduced simultaneously. To date, it remains a challenge to synthesize a N-doped carbon material with single N configuration. Therefore, we turned to a single N species as the model in theoretical calculation, and studied the adsorption energies of reactants for NC1000 in acetylene hydrochlorination reaction.
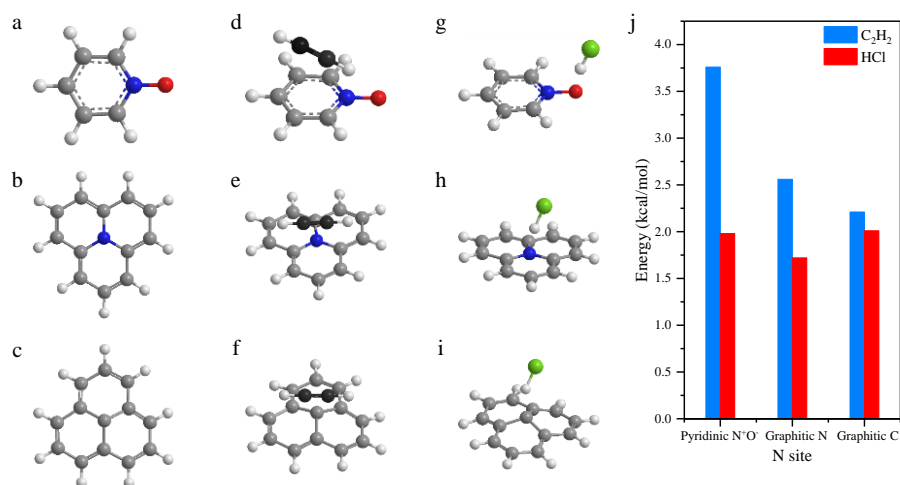
Fig. S3.3-1 The adsorption energies of C_2H_2 and HCl over pyridinic N^+O^-, graphitic N and graphitic C configurations.

The optimal adsorption structure and adsorption energies of C_2H_2 and HCl over graphitic N and pyridinic N^+O^- configurations of NC1000 were shown in Fig. S3.3-1. The adsorption energy of C_2H_2 over graphitic N and pyridinic N^+O^- configurations were -2.56 and -3.76 kcal/mol, respectively. For HCl, -1.72 and -1.98 kcal/mol were generated for graphitic N and pyridinic N^+O^- configurations. By comparing the adsorption energy results of substrates at different sites, it is clear that pyridinic N^+O^-, graphitic N and graphitic C have weaker ability to activate C_2H_2 and HCl than that of pyrrolic N and pyridinic N (Fig. S3.3-2), explaining the possible reasons for their low catalytic activity in Fig. 1d.
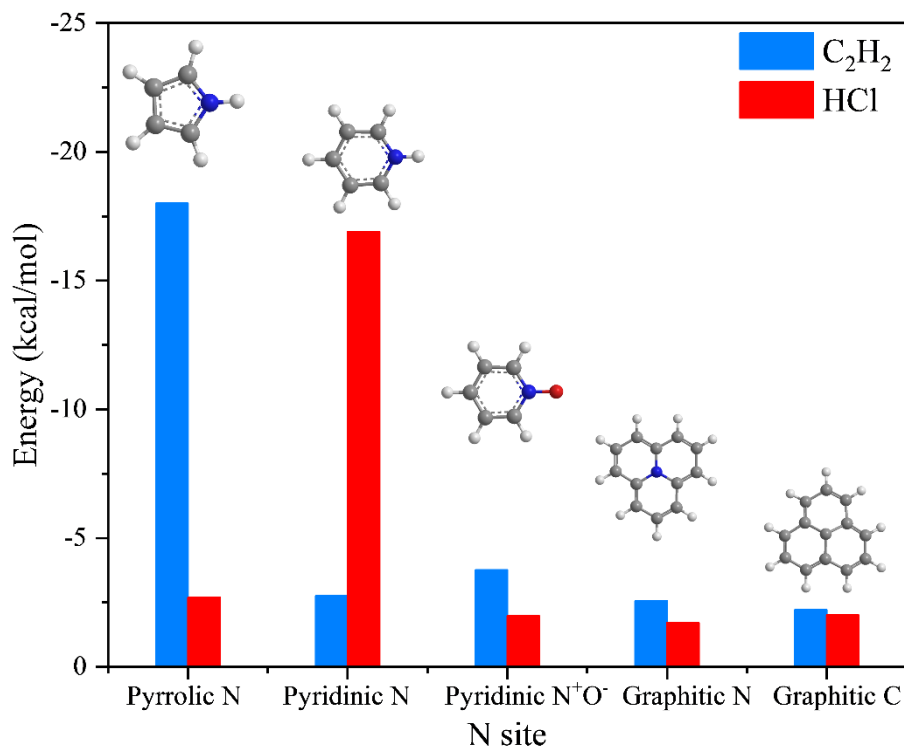
Fig. S3.3-2 The adsorption energies of C_2H_2 and HCl over different active sites.

Combined the adsorption energy of C_2H_2 and HCl, C_2H_2 preferentially adsorbed on N active site due to the lower adsorption energy of C_2H_2 compared to HCl. This result was consistent with the C_2H_2-TPD date (Fig. S3.1-1a). Furthermore, compared with the adsorption energy of C_2H_2 on the pyrrolic N site (existed on NC600-900 catalysts), its adsorption energy on graphitic N and pyridinic N^+O^- configurations is too weak to be comparable to the catalytic activity of NC600-900.

In summary, in this work, we will focus our research perspective on the pyrrolic N and pyridinic N sites instead of graphitic N and pyridinic N^+O^- configurations. However, the study of catalytic behavior of graphitic N and pyridinic N^+O^- configurations still has important theoretical and practical significance in acetylene hydrochlorination and target hydrohalogenation reactions.

4. Table and Figure captions

Table S1 The possible active site of nitrogen-doped carbon materials in acetylene hydrochlorination reaction.

Table S2 X-ray photoelectron spectroscopy (XPS) data of N 1s spectra of nitrogen-doped carbon materials from this work and other studies.

Table S3 Chemical compositions of the NC600, NC700 and NC900 from EDX.

Table S4 Textural properties of the NCT NC600, NC700, NC900 and NC1000).

Table S5 Comparison of reaction rate between catalysts developed in this work and other reported metal-free catalysts.

Table S6 Proposed reaction pathway of acetylene hydrochlorination.

Fig. S1 Reaction rate and N contents of NC600. NC700, NC900 and NC1000 catalysts.

Fig. S2 The adsorption energies of C_2H_2 and HCl over different N sites.

Fig. S3 Reaction rates and surface areas of NC600. NC700, NC900 and NC1000 catalysts.

Fig. S4 N1s XPS curve of NC700 evolution before and after acetylene hydrochlorination.

Fig. S5 MS signals of VCM for NC600, NC700 and NC900 under different reaction conditions.

Fig. S6 C_2H_2 and HCl TPD-MS of a-b) NC900, c-d) NC700 and e-f) NC600 under individual C_2H_2/HCl, and gas mixture of [C_2H_2 + HCl] pretreatment.

Fig. S7 Structures of pyrrolic N (blue ball, **Site 1-2**) and pyridinic N (red ball, **Site 3-**

5); and the adsorption energy of C_2H_2 and HCl over different N sites.

Fig. S8 Adsorption of C_2H_2 and HCl over dual-pyrrolic- and pyridinic N sites: a) Site a and b) Site b. c) Adsorption energies. Pyrrolic N (blue ball) and pyridinic N (red ball).

Fig. S9 The surface area (S_{BET}) of NC600, NC700 and NC900 at fresh, Stage 1 and Stage 2.

Fig. S10 The C/N and Cl/N ratio of NC600, NC700 and NC900 at fresh, Stage 1 and Stage 2.

Fig. S11 FTIR spectrum of the spent NCT (NC600, NC700 and NC900) and Pyridine hydrochloride.

Table S1 The possible active site of nitrogen-doped carbon materials in acetylene hydrochlorination reaction.

Catalyst	Active site	Ref.
SiC@NC	Pyrrolic N	S3
PDA/SiC	Pyrrolic N	S4
PANI-AC	Pyrrolic N	S5
N-Carbon	C atoms bond to pyridinic N	S6
ZIF-8/SAC	Pyrrolic N	S7
S,N-C	Pyrrolic N	S8
NS-C-NH$_3$	C atoms bond to pyridinic N	S9
g-C$_3$N$_4$-Cu/AC	Pyrrolic N	S10
g-C$_3$N$_4$/AC	Pyridinic N	S11
p-BN	Pyridinic N	S12
Z$_4$M$_1$	Pyrrolic N	S13
B, N-G	Pyrrolic N	S14

Table S2 X-ray photoelectron spectroscopy (XPS) data of N 1s spectra of nitrogen-doped carbon materials from this work and other studies.

| Sample | Pyridinic N [a] | | | Pyrrolic N [a] | | | Graphitic N [a] | | | Pyridinic N$^+$O$^-$ [a] | | | Ref. |
| | Position/ | FWHM[b]/ | Area/ | Position/ | FWHM[b]/ | Area/ | Position/ | FWHM[b]/ | Area/ | Position/ | FWHM[b]/ | Area/ | |
	eV	eV	%	eV	eV	%	eV	eV	%	eV	eV	%	
NC1000	--	--	--	--	--	--	401.3	1.5	88.15	403.3	2.0	11.85	This work
NC900	398.3	1.7	9.3	--	--	--	401.1	2.3	80.5	403.3	1.8	10.2	This work
NC700	398.3	1.50	38.0	400.01	1.53	22.0	401.1	1.59	30.5	403.3	2.50	7.4	This work
NC600	398.2	1.51	32.1	400.09	1.53	15.6	401.0	1.60	43.7	403.3	2.56	8.6	This work
NC1-1073	398.3	1.51	35.8	400.2	1.45	35.7	401.1	1.31	22.4	403.3	1.68	6.1	S15
NC	398.3	1.5	23.7	400.5	2.2	40.0	401.2	2.0	28.1	403.3	1.7	8.2	S15
NC-573	398.5	1.51	33.3	400.4	1.99	37.6	401.2	2.06	22.5	400.3	1.68	7.8	S15
NC-973	398.5	1.69	36.1	400.4	1.96	24.7	401.2	1.51	29.2	403.3	2.44	9.9	S15

[a] based on reference values; [b] FWHM = full width at half maximum.

Table S3 Chemical compositions of the NC600, NC700 and NC900 from EDX.

Stage	Sample	C (*wt.*%) [a]	N (*wt.*%) [a]	O (*wt.*%) [a]	Cl (*wt.*%) [a]	Carbon mass balance (*wt.*%) [b]
Fresh	NC900	77.2	18.5	4.3	0	100
	NC700	75.6.	19.9	4.5	0	100
	NC600	70.2	24.6	5.2	0	100
Stage 1	NC900	75.2	16.9	3.3	4.6	> 98.8
	NC700	70.8	19.5	5.5	4.2	> 98.7
	NC600	69.8	21.7	3.1	5.4	> 98.5
Stage 2	NC900	--	--	--	--	--
	NC700	85.9	9.4	2.1	2.6	> 83.2
	NC600	87.3	8.9	1.9	2.5	> 86.9

[a] The identification and determination of the element content here does not use XPS technology, since XPS is a surface analysis technology that does not adequately reflect the bulk phase information of the evaluated sample. Therefore, EDX is selected as a bulk phase analysis technique.

[b] The carbon balance can be obtained by comparing the moles of carbon accounted for in unreacted acetylene and in the identified products to the moles of carbon in acetylene entering the reactor.

Table S4 Textural properties of the NCT NC600, NC700, NC900 and NC1000).

Sample	S_{BET} (m^2 g^{-1}) [a]	Volume (cm^{-3} g^{-1}) [b]	Diameter (nm) [c]
NC1000	575	0.37	1.12
NC900	826	0.45	1.19
NC700	789	0.39	1.15
NC600	672	0.34	1.14

[a] measured using the Brunauer-Emmett-Teller (BET) method; [b] calculated dependent on the adsorbed N_2 volume; [c] determined by Barrett-Joyner-Halenda (BJH) method.

We can see that high surface area was obtained due to the self-assembly of ILs in the carbonization process. During the thermal decomposition of the IL mixtures, $[NTf_2]^-$ anions are polymerized to form ionic clusters with the neighboring counter cations (such as $EMIM^+$-$[EMIM^+$-$NTf_2^-]_2$, NTf_2^--$[EMIM^+$-$NTf_2^-]_2$, and $[EMIM^+$-$NTf_2^-]_2$) with different sizes. Ionic clusters sizes of $EMIM^+$-$[EMIM][NTf_2]_2$, NTf_2^--$[EMIM][NTf_2]_2$, and $[EMIM][NTf_2]_2$ were centered at 0.9-3.2 nm. When the ionic clusters are trapped in the carbon matrix, they acted as a porogen, which was responsible for the pore formation in the carbonization process. Similar results have been studied in our previous work [S16].

Table S5 Comparison of reaction rate between catalysts developed in this work and other reported metal-free catalysts.

Sample	Temp. (°C)	GHSV(C_2H_2) (h^{-1})	Reaction rate ($mol_{C_2H_2}h^{-1}kg_{Cat}^{-1}$)	Ref.
SiC@NC [a]	200	30	1.95	S3
PDA/SiC [a]	200	--	5.46	S4
PANI-AC [a]	180	36	3.12	S5
NC(ZIF-8) [a]	220	30	3.31	S6
NS-C-NH3 [a]	220	35	13.26[a]	S9
C_3N_4/AC [a]	180	50	3.97	S11
p-BN [a]	280	44	3.31	S12
B,N-G [a]	150	36	2.38	S14
NC1000 [b]	180	90	0.13	This work
NC900 [b]	180	90	2.39	This work
NC700 [b]	180	90	5.94	This work
NC600 [b]	180	90	4.96	This work

[a] Reaction rate was carried out with a gas pressure of 1 kPa. The reaction rate is calculated as the molar amount of acetylene converted per kilogram of catalyst per hour ($mol_{C_2H_2}h^{-1}kg_{Cat}^{-1}$). [b] Reaction rate was carried out in this work and the presence of internal and external mass transfer limitations were excluded using the Weisz-Prater and Mears criterion (section 2 of *Supporting Information*). The VCM selectivity for all evaluated catalysts were over 98%.

We can see that the reaction rate of NC700 was lower than the reported NS-C-NH3 but higher than other reported catalysts even at the same temperature and higher GHSV.

Table S6 Proposed reaction pathway of acetylene hydrochlorination.

Pathway 1[a]		Pathway 2[b]		Pathway 3[c]	
Eley-Rideal mechanism		Eley-Rideal mechanism		Langmuir-Hinshelwood mechanism	
Step	Description	Step	Description	Step	Description
Adsorption	$* + C_2H_2 \leftrightarrow *C_2H_2$	Adsorption	$* + HCl \leftrightarrow *HCl$	Adsorption	$* + C_2H_2 \leftrightarrow *C_2H_2$ $* + HCl \leftrightarrow *HCl$
Reaction	$HCl + *C_2H_2 \leftrightarrow C_2H_3Cl*$	Reaction	$C_2H_2 + *HCl \leftrightarrow C_2H_3Cl*$	Reaction	$* C_2H_2 + *HCl \leftrightarrow C_2H_3Cl* + *$
Desorption	$C_2H_3Cl* \leftrightarrow C_2H_3Cl + *$	Desorption	$C_2H_3Cl* \leftrightarrow C_2H_3Cl + *$	Desorption	$C_2H_3Cl* + * \leftrightarrow C_2H_3Cl + * + *$

* adsorption site.

[a] The reaction can be triggered by the reaction of C_2H_2 adsorbed on the active N site with gaseous HCl to form vinyl chloride.

[b] The reaction can be triggered by the reaction of HCl adsorbed on the active N site with gaseous C_2H_2 to form vinyl chloride.

[c] The reaction can be triggered by the reaction of C_2H_2 and HCl adsorbed on the active N site to form vinyl chloride.
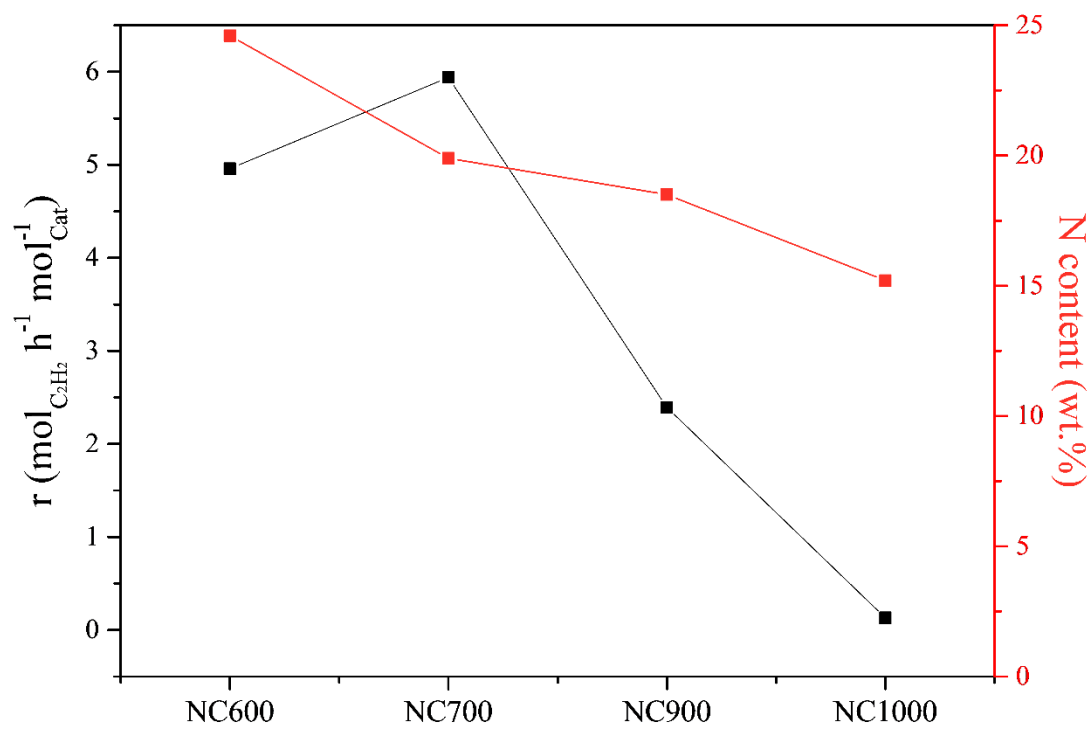
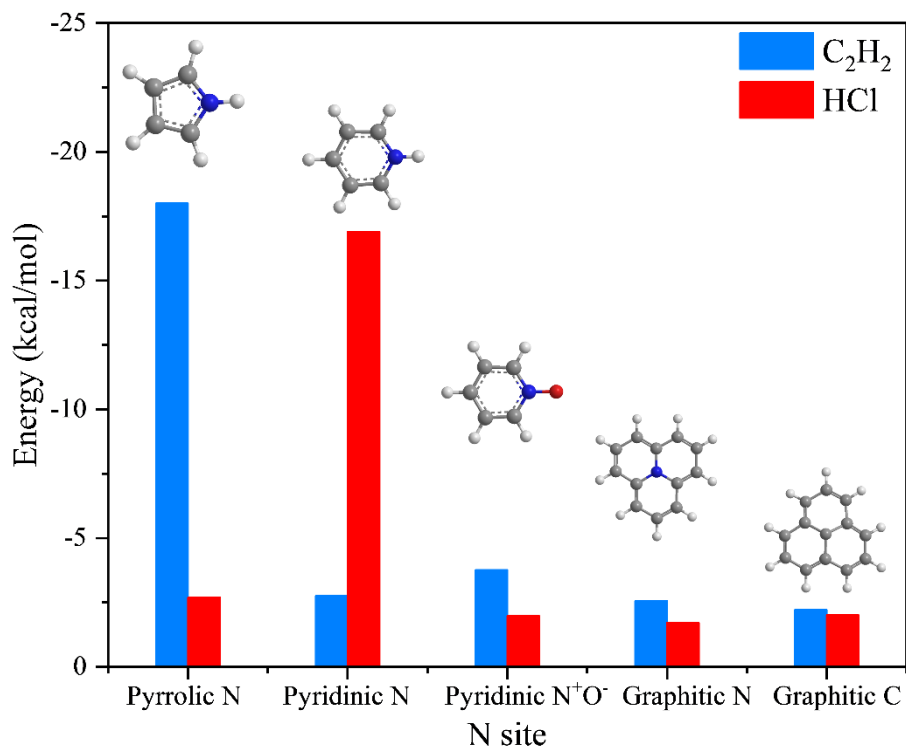Fig. S1 Reaction rate and N contents of NC600. NC700, NC900 and NC1000 catalysts.

Fig. S2 The adsorption energies of C_2H_2 and HCl over different N sites.

By comparing the adsorption energy results of substrates at different sites, it is clear that pyridinic N^+O^-, graphitic N and graphitic C have weaker ability to activate C_2H_2 and HCl than that of pyrrolic N and pyridinic N, explaining the possible reasons for their low catalytic activity in Fig. 1d. Since pyridinic N^+O^-, graphitic N and graphitic C have the lowest ability to activate substrates, when the reaction gas mixture flows through the catalyst bed, the substrate tends to be activated at pyrrolic N and pyridinic N.
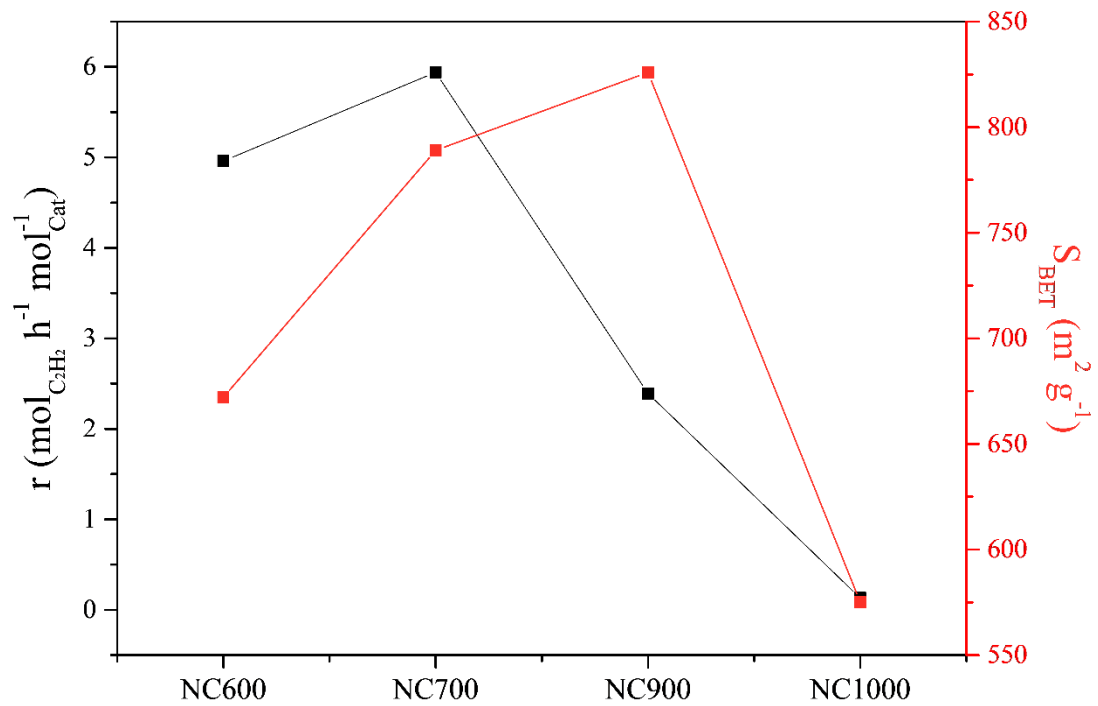
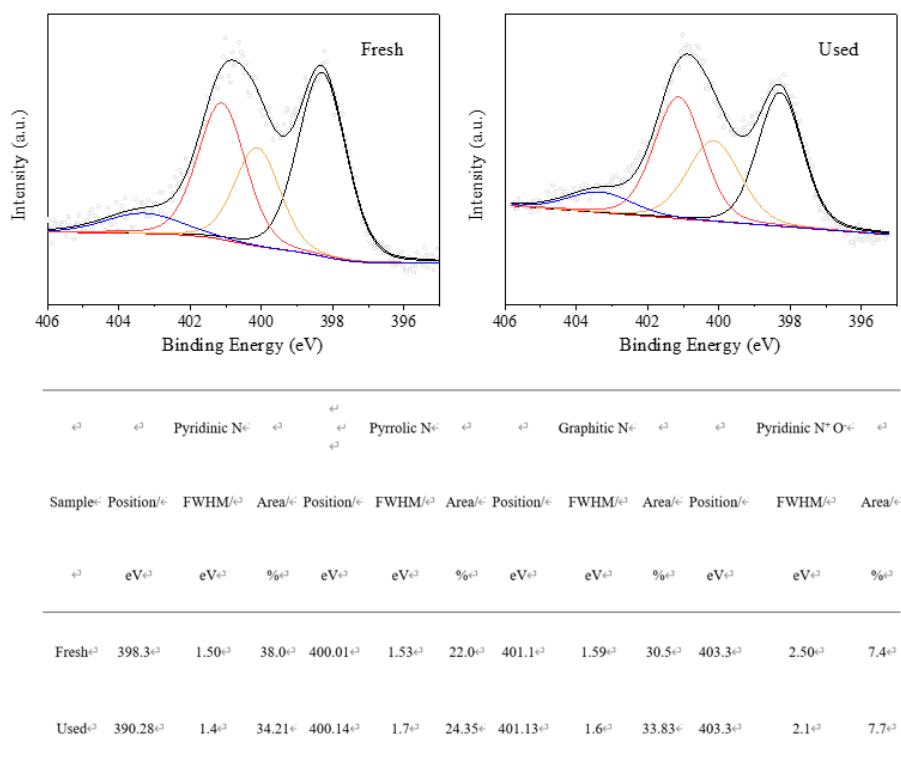Fig. S3 Reaction rates and surface areas of NC600. NC700, NC900 and NC1000 catalysts.

	Pyridinic N			Pyrrolic N			Graphitic N			Pyridinic N⁺O⁻	
Sample	Position/	FWHM/	Area/	Position/	FWHM/	Area/	Position/	FWHM/	Area/	Position/	FWHM/	Area/
	eV	eV	%	eV	eV	%	eV	eV	%	eV	eV	%
Fresh	398.3	1.50	38.0	400.01	1.53	22.0	401.1	1.59	30.5	403.3	2.50	7.4
Used	390.28	1.4	34.21	400.14	1.7	24.35	401.13	1.6	33.83	403.3	2.1	7.7

Fig. S4 N1s XPS curve of NC700 evolution before and after acetylene hydrochlorination.

The nitrogen-doped carbon material synthesized in this work is chemically stable at the evaluated reaction temperature because the nitrogen configurations on the material surface are obtained by heat treatment at a temperature of at least 600 °C. Among the evaluated catalysts, NC700 is the most active and stable catalysts. Therefore, we select the NC700 sample as an example to study the chemical stability of nitrogen configurations during reaction process. The Fig. S4 shows that the coincidence of the N1s curve before and after the reaction, suggesting the nitrogen configurations did not change during the reaction. In other words, the phenomenon of pyrrolic- and pyridinic N converted to other types N can not been occurred during the catalysis process of this work.
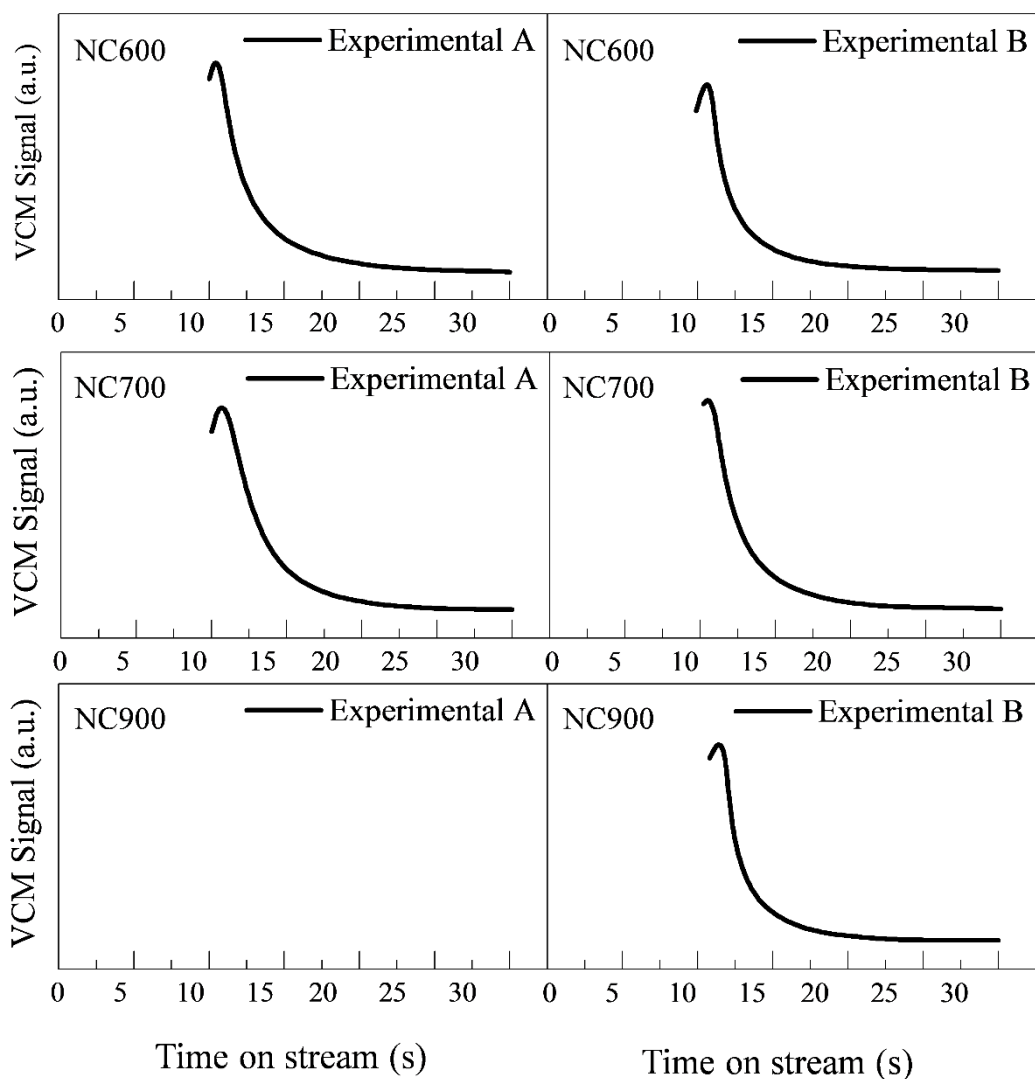
Fig. S5 MS signals of VCM for NC600, NC700 and NC900 under different reaction conditions.

Experiental A: C_2H_2 (30 min) $\rightarrow$ N_2 (60 min) $\rightarrow$ HCl $\rightarrow$ VCM Signal

Experiental B: HCl (30 min) $\rightarrow$ N_2 (60 min) $\rightarrow$ C_2H_2 $\rightarrow$ VCM Signal

In experimental A (**B**), the evaluated sample was first pre-treated with C_2H_2 (**B, HCl**) under reaction conditions for 30 min, followed by N_2 purging for 60 min to remove the physically adsorbed C_2H_2 (**B, HCl**) residual in the catalyst bed. Subsequently, HCl (**B, C_2H_2**) was introduced into the catalyst bed to detect the signal of VCM.

Fig. S6 C_2H_2 and HCl TPD-MS of a-b) NC900, c-d) NC700 and e-f) NC600 under individual C_2H_2/HCl, and gas mixture of $[C_2H_2 + HCl]$ pretreatment.
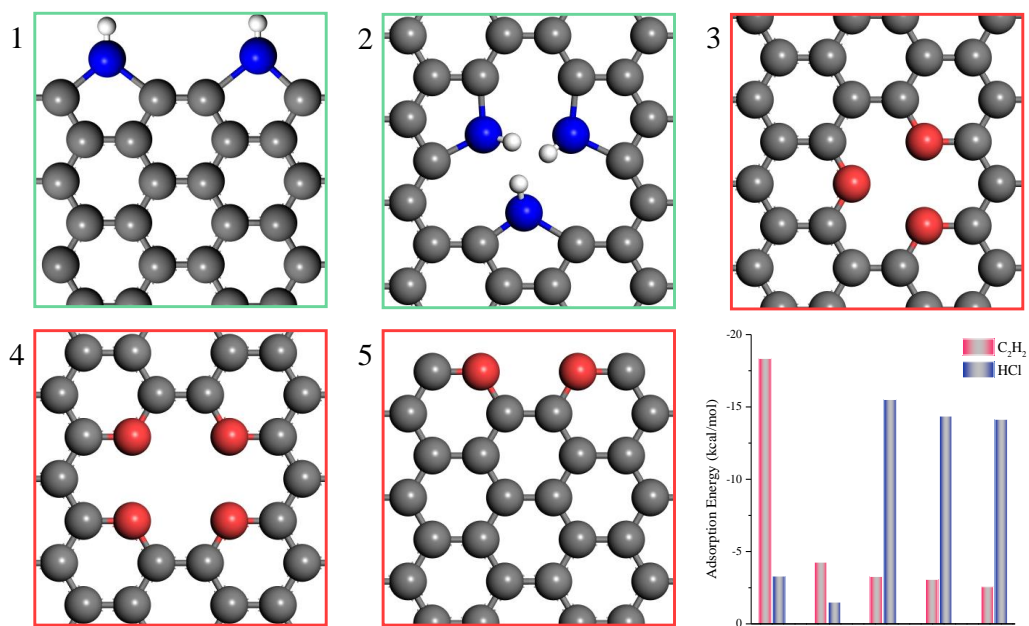
Fig. S7 Structures of pyrrolic N (blue ball, **Site 1-2**) and pyridinic N (red ball, **Site 3-5**); and the

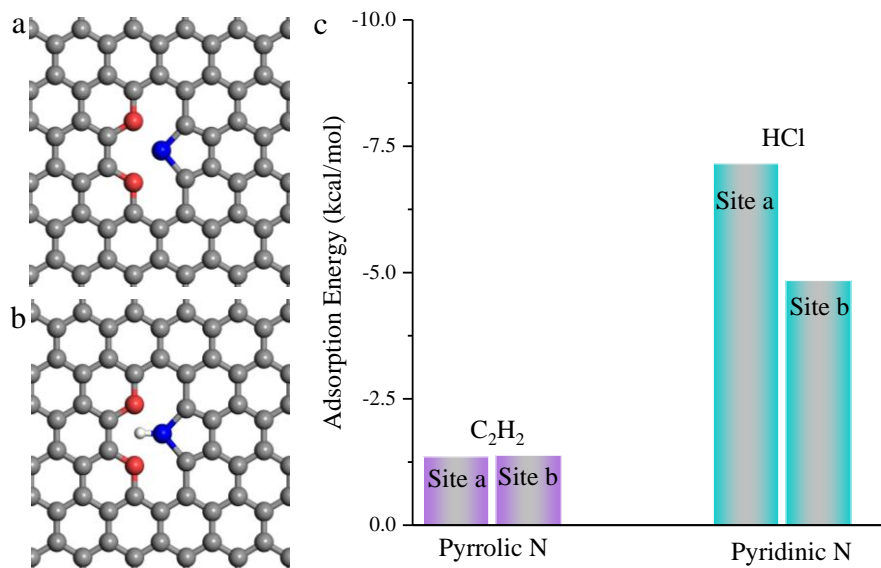adsorption energy of C_2H_2 and HCl over different N sites.

Fig. S8 a-b) Distribution states of dual-[pyrrolic- + pyridinic N] at site (a) and site (b). Pyrrolic N

(blue ball) and pyridinic N (red ball); c) Adsorption energies of C_2H_2 and HCl over dual-pyrrolic-
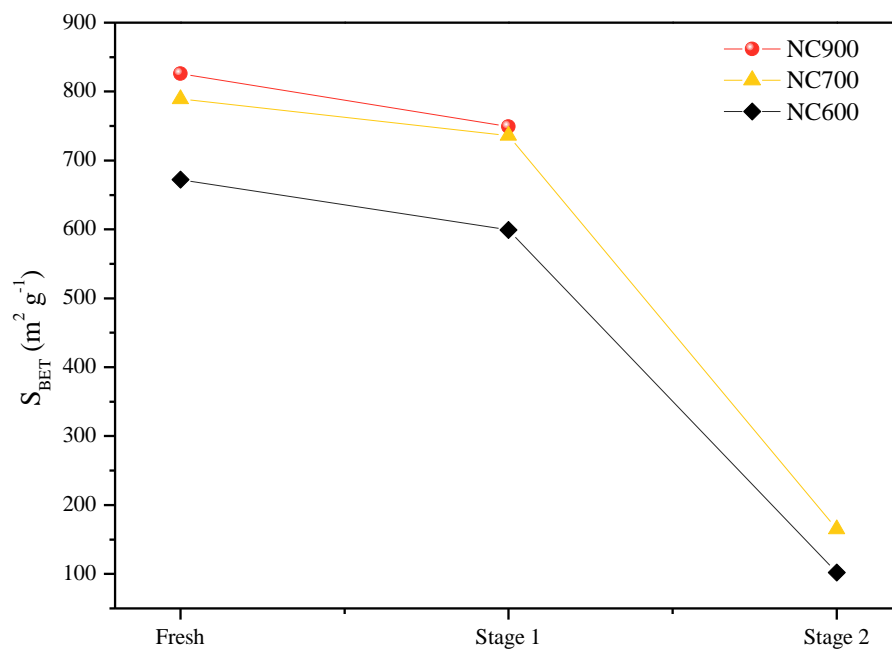
and pyridinic N sites: a) Site a and b) Site b.

Fig. S9 The surface area (S_{BET}) of NC600, NC700 and NC900 at fresh, Stage 1 and Stage 2.
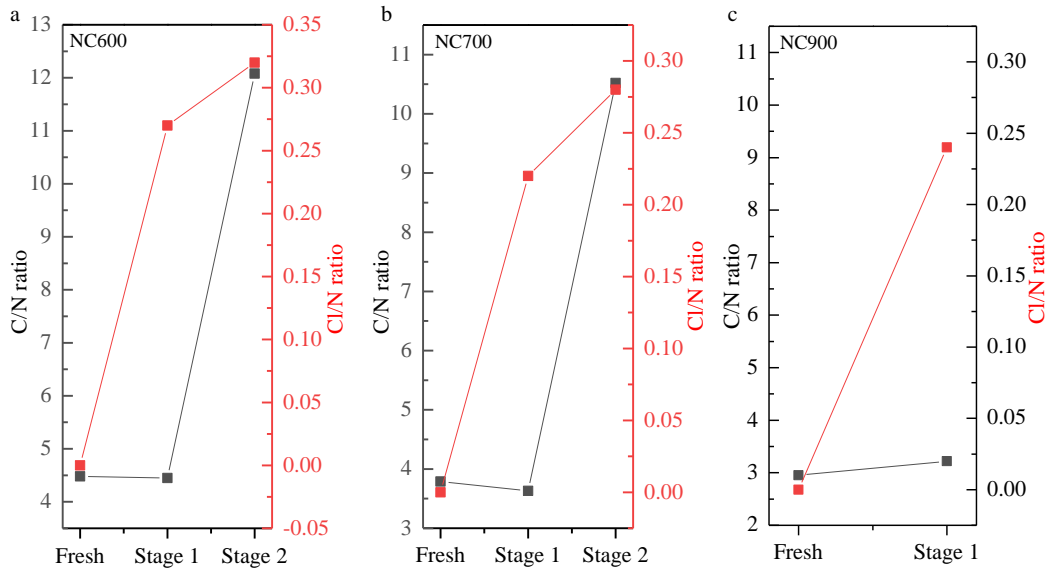
Fig. S10 The C/N and Cl/N ratio of NC600, NC700 and NC900 at fresh, Stage 1 and Stage 2.
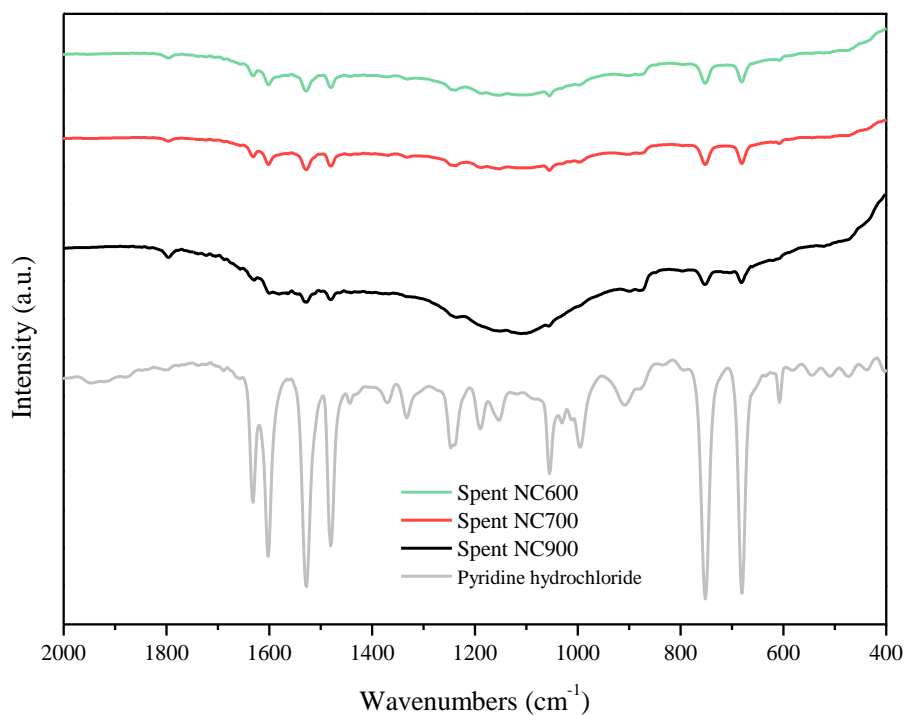
Fig. S11 FTIR spectrum of the spent NCT (NC600, NC700 and NC900) and Pyridine hydrochloride.

Fig. S11 shows that the coinciding characteristic peaks could be found between the spent NCT and Pyridine hydrochloride (Aladdin Reagent), which suggests that pyridine hydrochloride-like salts has been produced during acetylene hydrochlorination.

References

S1. H.S. Fogler, Elements of Chemical Reaction Engineering, *Prentice Hall Professional Technical Reference*, 2006.

S2. R. Perry, D. Green, Perry's Chemical Engineers' Handbook, Eighth Edition, *McGraw-Hill Education*, 2008.

S3. 10   X. Y. Li, X. L. Pan, L. Yu, P. J. Ren, X. Wu, L. T. Sun, F. Jiao, X. H. Bao, *Nat. Commun*., 2014, 5, 3688-3694.

S4. X. Y. Li, P. Li, X. L. Pan, H. Ma, X. H. Bao, *Appl. Catal., B*., 2017, 210, 116-120.

S5. C. Zhang, L. Kang, B. M. Zhu, B. Dai, *RSC Adv*., 2015, 5, 7461-7468.

S6. S. Chao, F. Zou, F. Wan, X. Dong, Y. Wang, Y. Wang, Q. Guan, G. Wang, W. Li, *Sci. Rep*., 2017, 7, 39789.

S7. X. Li, J. Zhang, Y. Han, M. Zhu, S. Shang, W. Li, J. *Mater. Sci*., 2018, 53, 4913-4926.

S8. J. Wang, F. Zhao, C. Zhang, L. Kang, M. Zhu, *Appl. Catal. A: Gen*., 2018, 549, 68-75.

S9. X. Dong, S. Chao, F. Wan, Q. Guan, G. Wang, W. Li, *J. Catal*., 2018, 359, 161-170.

S10. W. Zhao, M. Zhu, B. Dai, *Catalysts*, 2016, 6, 193.

S11. X. Li, Y. Wang, L. Kang, M. Zhu, B. Dai, *J. Catal*., 2014, 311, 288-294.

S12. P. Li, H. B. Li, X. L. Pan, K. Tie, T. T. Cui, M. Z. Ding, X. H. Bao, *ACS Catal*., 2017, 7, 8572-8577.

S13. X. Li, J. Zhang, W. Li, *J. Ind. Eng. Chem*., 2016, 44, 146-154.

S14. B. Dai, K. Chen, Y. Wang, L. Kang, M. Zhu, *ACS Catal*., 2015, 5, 2541-2547.

S15. R. Lin, S.K. Kaiser, R. Hauert, J. Pérez-Ramírez, *ACS Catal*., 2018, 8, 1114-1121.

S16. J. Zhao, B. Wang, Y. Yue, G. Sheng, H. Lai, S. Wang, L. Yu, Q. Zhang, F. Feng, Z. Hu, X. Li,

J. Catal., 2019, 373, 240-249.